

# **CFD SIMULATIONS TO DETERMINE THE EFFECTS OF DEFORMATIONS ON LIQUID METAL COOLED WIRE WRAPPED FUEL ASSEMBLIES**

**Eugeniy Sosnovsky**

Varian Medical Systems  
6659 Kimball Drive, Suite E-502, Gig Harbor, WA 98335, USA  
Eugeniy.Sosnovsky@varian.com

**Emilio Baglietto**

Department of Nuclear Science and Engineering, Massachusetts Institute of Technology  
77 Massachusetts Ave, Cambridge, MA 02139, USA  
emiliob@mit.edu

**Steven Keijers, Katrien van Tichelen**  
SCK•CEN, Mol, Belgium

**Thiago Cardoso de Souza, Heleen Doolaard and Ferry Roelofs**  
NRG, Petten, Netherlands

## **ABSTRACT**

Over the course of their lifespan, wire-wrapped liquid metal fast reactor (LMFR) fuel bundles deform due to tension of the pre-stressed wires, contact pressure between clad and adjacent rods' wires, thermal and irradiation clad creep, irradiation-caused swelling and fuel burnup. This deformation is geometrically complex, because it is the result of multiple effects, most of which do not arise until after burnup. This deformation affects both the axial flow areas and the crossflow mass fluxes, which have an effect on the subchannel outlet temperatures – a limiting parameter in many LMFRs.

This paper aims to identify and quantify the effects of deformations on the heat transport in LMFR fuel assemblies. To achieve this, a 19-pin and a 127-pin hexagonal wire-wrapped fuel bundles are simulated in nominal and deformed geometries, using deformations of varying fidelity. A thorough CAD deformation algorithm is developed and presented; this algorithm generates a realistic solid model of a deformed LMFR fuel bundle, with a deformation shape similar to shapes observed experimentally. This algorithm is applied to the 19-pin bundle. The results of the simulations of the 19-pin bundle, together with its CAD deformation algorithm, are used to develop a methodology that core designers could use to quantify the hot channel penalty factors due to bundle deformation with a set of CAD and CFD codes.

The CFD-based hot subchannel deformation penalty factor quantification methodology was tested by applying it to the 19-pin bundle experiment. For this benchmark, the penalty factor was evaluated to be 5.8%. Additional results presented in the paper include a study of the effects of deformations on the outlet fluid temperatures in both the 19-pin and the 127-pin assemblies.

## **KEYWORDS**

CFD, LMFR, deformations, penalty factor

## 1. INTRODUCTION

The initial work in CFD simulations of nominal LMFR fuel assemblies is relatively recent, due to the high complexity of wire-wrapped geometries, which require large meshes to be accurately simulated. A recent overview can be found in Ref. [1]. There exist several verification and validation (V&V) studies on turbulence and boundary layer models for CFD simulations of nominal LMFR fuel assemblies; the ones relied upon in this work suggest using the standard  $k-\varepsilon$  turbulence model with a high  $y^+$  wall treatment for sodium [2], and the  $k-\omega$  SST model for lead-bismuth eutectic (LBE) [3]. Both studies also suggest specific geometric simplifications to the wrapping wire shapes, which greatly reduce the number of cells required to adequately mesh the rod-wire contact interfaces, without significantly impacting accuracy.

Reference [2] in particular relied on a 19-pin wire-wrapped electrically-heated assembly experiment, conducted at Oak Ridge National Laboratory in the 1970s [4]. Only nominal geometries were constructed and measured in this and other similar experiments, and the models above were therefore only verified and validated for these nominal, undeformed geometries with straight cylindrical pins and flat hexagonal ducts. However, even before the fuel enters the reactor, the wire winding process introduces a pre-stress in the wire and the rod, which results in the rod itself wrapping around the wire. LMFR fuel then further deforms over the course of its lifespan, as a result of the contact pressure between its clad and adjacent rods' wires, thermal and irradiation clad creep, irradiation-caused swelling and fuel burnup. This deformation of LMFR fuel can degrade its cooling, particularly after burnup, and must therefore be accounted for in core design. In this paper, we rely on the models and geometric simplifications verified and validated for nominal geometries, to simulate deformed geometries; we therefore implicitly assume that the deformed geometries are not sufficiently different from the nominal ones to invalidate the models.

The simulations of the 127-pin geometry described in this paper are preparatory work in the licensing process of the Multi-purpose hYbrid Research Reactor for High-tech Applications (MYRRHA), currently under design at SCK•CEN [5]. The purpose of this preparatory work is to identify the effects of deformations of a fuel assembly at limited burnup on the cooling and heat transport, compared to the simplified straight cylindrical pin models. MYRRHA is a flexible fast spectrum research reactor cooled by LBE. MYRRHA is identified as the European Technology Pilot Plant for the Lead Cooled Fast Reactor (LFR), which is one of the Generation IV reactor concepts [6]. As most liquid metal cooled fast reactors, MYRRHA also employs wire-wrapped fuel bundles.

The deformed geometries of each individual pin in a burnt-up fuel bundle are unique, due to the fact that some of the deforming effects listed above are a function of the pin's position, and individual variations. A typical deformation can be described as follows though: the clad radially strains (non-uniformly, axially), and the wrapping wire, while it does undergo radiation strain, does not generally expand to the same degree, and so the axial stress induced by the wire increases. This results in the rod itself slowly wrapping itself more and more around the wire. This deformation mechanism was observed and documented in a number of experiments [7,8].

To assess the influence of the combined-effect (i.e., end-of-life) deformations on LMFR fuel using CFD, it is necessary to: (a) build CAD models of both the nominal and deformed geometries, (b) simulate each model using a CFD code under similar physical assumptions, and (c) compare the simulation results. Part of the challenge arises from the fact that deformed geometries are very complex, and are not easily parametrized: the resulting geometry is a balance of several effects which apply differently shaped strains on the fuel. Early attempts at reproducing the deformed geometries modeled a radially strained hexagonal duct with radially strained and bowed pins [9]. The above-referenced experimental studies on real deformed wire-wrapped fuel assemblies have shown, that the resulting "onion-type" geometry does not closely match experiment: as stated above, deformed rods tend to wrap themselves around the wires ("twist"), instead of simply bowing harmonically (i.e., half-sinusoidally) to one side. It would be

prohibitively expensive to run irradiation experiments to obtain a deformed geometry for every fuel assembly type (particularly at the design stages), therefore there is room for improvement in the CAD procedures used to construct the deformed geometries, which part of this work seeks to address.

Further, simulating multiple deformed geometries for every assembly in the design space is, again, prohibitively expensive; so is relying exclusively on CFD for thermal hydraulic reactor simulations. We therefore intend to provide a clear methodology to LMFR assembly designers, which could be applied to quantify penalty factors. Such penalty factors could then be introduced into subchannel and even systems-level thermal hydraulic codes, thereby accelerating the composition of thermal hydraulic simulations on which initial LMFR reactor design processes rely. Such methodology is another result of this work.

Section 2 of this paper presents two deformation procedures: a simpler uniformly twisted and radially strained one, and a non-uniformly twisted and radially strained one. The second procedure is more complex, and is intended to closely match the experimentally obtained deformations at higher burnup. The two procedures are applied to a 127-pin and a 19-pin fuel assemblies, respectively; the CFD models and assemblies used are described in section 3. The more complex, non-uniform deformation procedure is used as the basis of a hot channel deformation penalty factor evaluation methodology, developed in section 4. The results of the CFD simulations of the two assemblies with and without deformations are given in section 5; conclusions and future work are summarized in section 6.

## 2. NOMINAL AND DEFORMED GEOMETRIES DESCRIPTION

A typical hexagonal LMFR assembly consists of a triangular lattice of wire-wrapped cylindrical rods, inside a hexagonal duct. The hexagonal duct geometry is trivial to model; there are, however, two different ways to build a CAD model of a nominal wire-wrapped cylindrical rod, described below. Here, a “nominal rod” is assumed to be a straight cylinder. This is a simplifying assumption: some of the initial deformation can occur purely due to the wire pre-stress; this is acceptable, as the deformation only gets worse over fuel lifetime. Throughout this work, SolidWorks 2014 x64 is used to build the CAD models for the 19-pin bundle, for which the deformation algorithm is described in more detail, and so SolidWorks terminology is used. Other CAD packages generally have similar features, although the terminology may vary.

The first way to wrap a wire around a cylindrical extrusion is to:

1. Construct a helical path (using the “Helix and Spiral” tool) around the rod centerline.
2. Construct a circular cross section for the wire, on the bottom *horizontal plane*. Add the radial simplifications to reduce the cell count (described below).
3. Sweep the cross-section along the helical path, using the Swept Boss/Base tool.

The geometric approximation in this approach is that the wire’s cross section at all times remains perfectly horizontal, and *not* normal to the helical path, which it is in the real geometry. This is because of the configuration of the sweep and the orientation of the plane on which the sweep profile sketch is created.

With correct rod dimensions, this problem is barely noticeable: the angle between the wire path normal plane and the horizontal plane is very small, and so the variation in the wire sweep is sufficiently small to be ignored. For example, for the 19-pin ORNL geometry (36” rods with 3 full wire turns), the angle between the two planes is only 4.31°. Still, this approximation is unnecessary, and can be removed without impacting the model’s complexity.

The second way to wrap a wire around a cylindrical extrusion is to:

1. Construct a helical path (using the “Helix and Spiral” tool) around the rod centerline.
2. Using the “Pierce” constraint, construct a plane normal to the helix at the base of the rod.
3. Sketch the wire cross section (simplified as discussed below) on the helix-normal plane.
4. Again using the Swept Boss/Base tool, construct the wire using the sketched cross section as the sweep profile, the helical path as the sweep path, and the rod centerline as the 1<sup>st</sup> guide curve.

In the resulting geometry, the sweeping wire will always remain normal to the helical path, as the case in the physical geometry.

Figure 1 below illustrates the two different ways to model the wire described above.

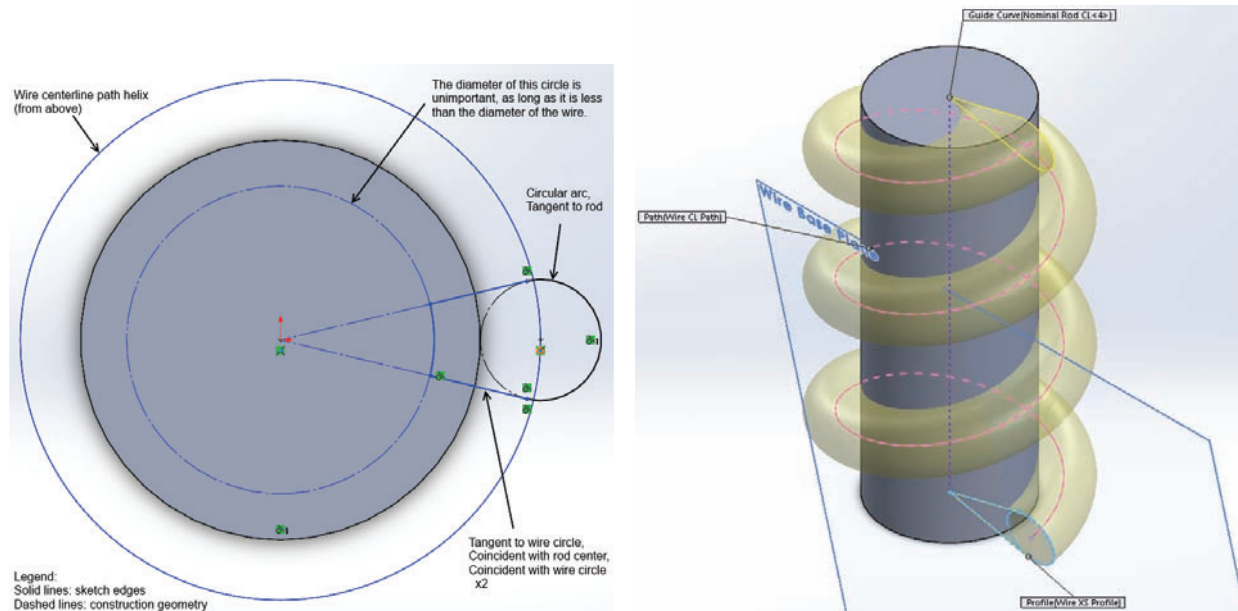


**Figure 1. Wire Modeling Techniques Using Horizontal (left) and Normal (right) Cross-Sectional Sweep Profiles (not to scale)**

Note, that the wire cross section is modeled as a triangular radial-sided wedge with a circular arc, and not as a perfect circle. This geometric simplification, mentioned above, has been validated in Ref. [2], in which CFD simulations with a more exact (nearly line contact), and a simplified (triangular radial-sided wedge with a circular arc, as above), clad-wire contact representations, were built and compared, and found to be in close agreement. This comparison has also been confirmed in earlier studies on the approximations for modeling wire wraps [10,11]. This simplification is very important: without simplifying the clad-wire contact, the mesher will need to somehow approximate the 1-dimensional (line) contact between the circular cross sections of the wire and the rod, which is likely to make it fail, and significantly increase the number of cells required.

The triangular radial-sided wedge with a circular arc representation of the wire cross section was used for the nominal and deformed versions of the 19-pin geometry. The clad-wire contact in the 127-pin geometry was represented using circular fillets of about 1/8 of the wire radius, on both sides of the contact line; it is illustrated in subsection 2.1.

The first wire-wrapping technique was used to model the rods in the non-deformed 127-pin geometry described in this paper. The second technique was used in the 19-pin geometry. The uniform twisted-and-radially-straining deformation was applied to the 127-pin geometry, described in subsection 2.1. The more

realistic non-uniform twisted-and-radially-straining deformation was applied to the 19-pin geometry, described in subsection 2.2.

## 2.1. Uniformly Twisted and Radially Strained Deformed Assembly CAD Model

In the analysis of the 127-pin geometry, a general set of deformations is considered in this work: namely, the pre-stressing effects of the wire-wraps on the fuel rods (“twist”), and the radial expansion of the fuel rods due to axially uniform thermal and irradiation effects (“radial strain”). Because the twist analyzed here results from the wire pre-stress, it is highly controlled, and is therefore assumed to be the same for every rod in the assembly. Similarly, the thermal expansion, which results in the radial strain of the wire and the clad, is also assumed to be axially uniform, and identical for all rods in the assembly.

The entire fuel assembly CAD geometry with 127 pins is modeled using ANSYS DesignModeler. To account for the mechanical deformations, fuel assemblies with deformed fuel rods were generated. A twist radius of 0.7mm was imposed on the rods. This value corresponds to the measured value of a fuel assembly mockup for pressure drop testing. For comparison, the nominal, undeformed geometry was also modeled as the reference case. As described above, the clad-wire contact was widened using circular fillets on both sides of the contact line, to avoid meshing problems. Figure 2 below illustrates a single rod out of this geometry; note the blue sweeping axis, 0.7mm offset from the rod centerline.

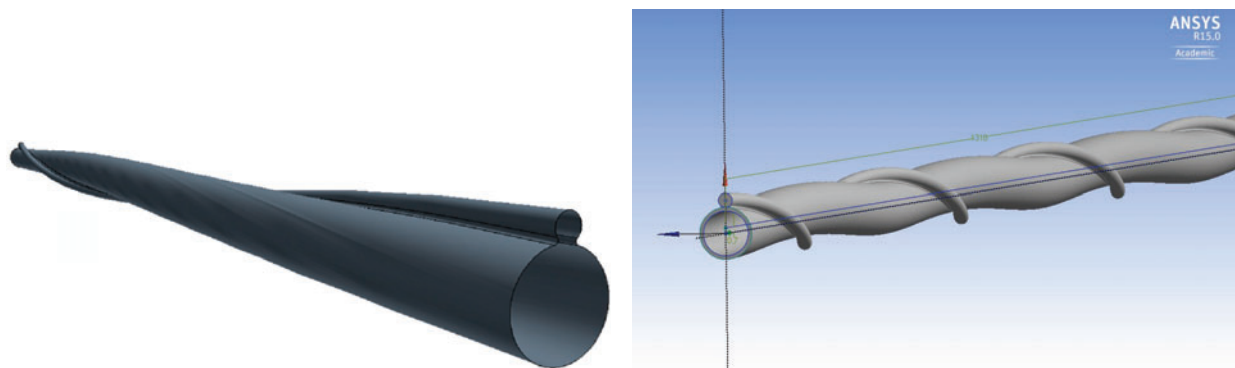


**Figure 2. One Streamwise Wire Pitch (left) and Three Pitches (right) of a Single Uniformly Twisted and Radially Strained Deformed Wire-wrapped Rod**

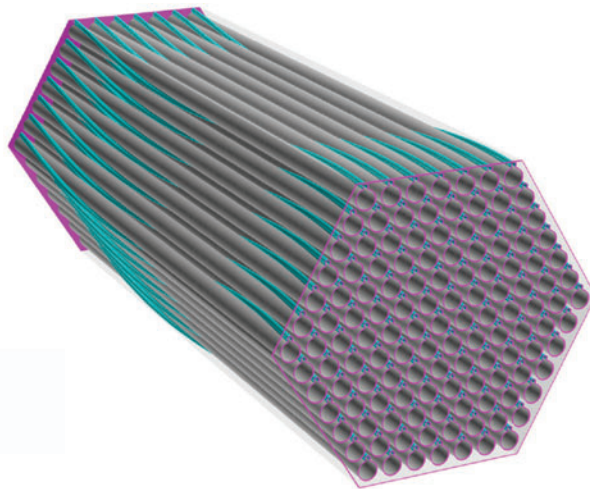


**Figure 3. 127-pin Wire-wrapped Fuel Assembly Geometry Consisting of 1 Streamwise Wire Pitch**

For the fuel bundle configuration, the pins are placed in a hexagonal housing (duct), such that the whole model of the fuel assembly consists of 5 full wire turns (itches). This includes both the active and the non-active axial regions. The nominal assembly is illustrated in Figure 3 above.

Due to the twisting effect imposed by the pre-stressed wires, the minimum distance between neighboring rods also reduces, which provides more horizontal free space for mounting the fuel rods in the bundle. To account for this phenomenon, two extreme cases are considered. In the first (“centric”) case, all pins are placed at the theoretical centered positions; in the second (“eccentric”) case, the pins are all compacted and shifted toward one side of the hexagon, and made to touch each other. The two cases are illustrated in Figure 4 below.

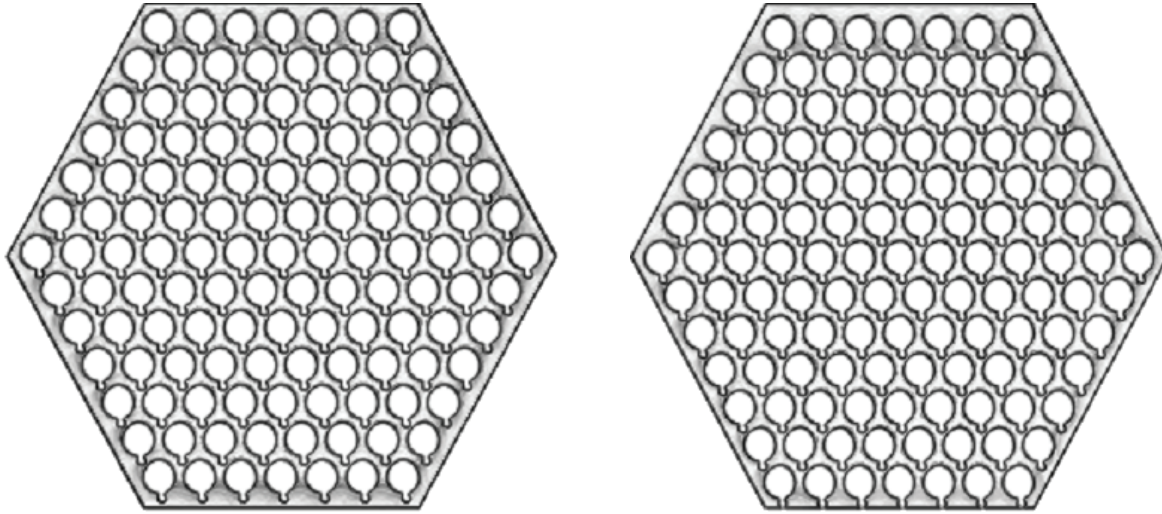


**Figure 4. Centric (left) and Eccentric (right) Fuel Bundle Placements in the Assembly Housing**

The 127-pin MYRRHA assembly was simulated using the meshing and physics models described in subsection 3.1; the simulation results are given in subsection 5.1.

## **2.2. Non-Uniformly Twisted and Radially Strained Deformed Assembly CAD Model Construction Procedure**

As was stated in section 1, the true deformation that a wire-wrapped rod experiences in an LMFR at high burnup does not look exactly like the uniformly radially strained and twisted rods in subsection 2.1. In real LMFRs, the end-of-life distortion is more complicated. Due to the effects summarized in section 1, the clad radially strains, which increases the axial tension applied by the wire. This results in the rod slowly bending (“wrapping”, or “twisting”) about the wire itself. References [7,8] illustrate this phenomenon experimentally: using X-ray techniques on burnt-up SFR fuel bundles revealed that the rods all wrap about their wires, with the radius of the rod’s wrap (in effect, the magnitude of the rod twist) increasing outward. There is therefore no onion-like radial expansion occurring in a true distorted SFR bundle, nor is the deformation the same in every rod. Instead, it is an assembly of helix-like rods, wrapped around their corresponding (helical) wires, with the degree of twist increasing radially outward.

The steps required to build a CAD model of this more complicated deformation can be summarized as follows:

1. A helical path is built for the rod; this is the path the rod lofts through. The helix’s diameter (aka “rod twist diameter”) is adjustable; it is most convenient to adjust the helix’s diameter using the SolidWorks External Equation File, in which named dimensions can be specified.

2. Nominally-sized rod cross-sectional profiles are built at the top and bottom of this helical path, on planes normal to the path (not horizontal!).
3. A radially expanded (by 1%) rod cross-sectional profile is built half way along this path. Note, that this suggests an axially non-uniform radial strain, seen in experiments [7,8].
4. A Loft feature connecting these three profiles is used to build the rod.
5. Steps 2-4, with wider (by the wire's diameter) cross-sectional profiles, are used to build the wire perimeter surface.
6. A twisted (turned) surface sweep is built around the rod path.
7. The intersection of surfaces built in steps 5 and 6 is a curve; this curve is used as the wire path.
8. Using way 2 described at the beginning of this section, and the triangular radial-sided wedge simplification of the clad-wire contact, the wire's cross-sectional sweep profile is built on the wire path-normal plane.
9. The rod's twist diameter can then be adjusted appropriately, to ensure that the rods do not overlap with their neighboring rods. This will result in the rod twist diameters increasing radially outward with each rod ring, which is, again seen in experiments [7,8].
10. The hexagonal duct is built using the Loft feature, assuming a radial strain that peaks in the middle.

An important property of this rather complicated algorithm is that with a radial strain of 0%, and a zero twist diameter, it completely matches the nominal geometry (with wires constructed using way 2) described at the beginning of this section. This is due to the fact that under these conditions, the rod path reduces to a straight vertical centerline, the wire perimeter surface of step 5 reduces to a cylinder, and the intersection of the turned surface of step 6 and the wire perimeter surface of step 5 therefore reduces to a perfect helix, which becomes the wire's path.

These steps are discussed in more detail below.

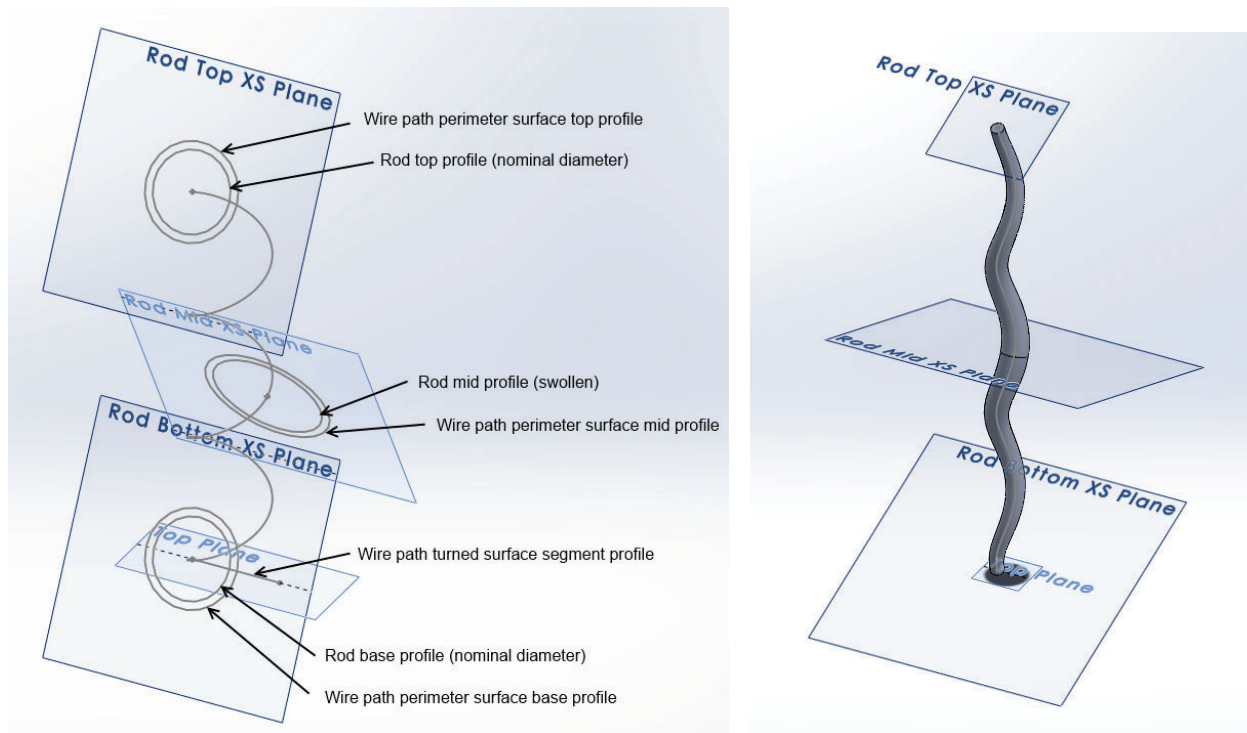


**Figure 5. Rod Path and Cross-Sectional Profiles (Steps 1-3) with Wire Path Perimeter Surface Cross-Sectional Profiles (Step 5, left) and Rod Body Loft Connecting the Profiles (Step 4, right) (not to scale)**

The helical path for the rod is simple to build; care must be taken, however, to orient this sweep in the same sense, but 180° out of phase, from the wire itself (as the wire and the rod, in effect, wrap “around” each other). In the illustrations below, looking downward, both the rod and the wire twist counterclockwise, 180° out of phase with each other.

The rod loft profiles and path are shown in Figure 5 above, on the left; these constitute steps 1-3 and part of 5 of the above procedure. The rod loft itself is shown on the right, which constitutes step 4. Note, that the deformations are grossly exaggerated, for clarity.

The wire path perimeter and twisted surfaces are illustrated in Figure 6 below; their intersection comprises the wire path, also in Figure 6. The wire sweep profile sketch is also shown on Figure 6. The deformations are again exaggerated for clarity.

Lastly, the wire is swept using the wire sweep profile and path from Figure 6, with the “Follow Path” orientation/twist type, “minimum twist” path alignment type, and using the rod centerline path from Figure 5 as the guide curve. The resulting wire-wrapped twisted and radially strained rod is shown in Figure 7.

The rod twist diameters are chosen to be the same for each rod ring, such that the resulting wire path length remains constant (within 1µm) for the center rod, and to maintain the distance between the adjacent rods for the outer rings. This results in a geometry consistent with the findings in Refs. [7,8]: the center rod experiences almost no twist, and the least twist of all of the rods in the assembly. The twist diameter gradually increases outward. Overall, the rods in the outermost rings end up being somewhat more twisted than they need to be (as in Refs. [7,8], while the most twisted rods are in the outermost ring, they are not all twisted completely uniformly), but this is a desirable, conservative assumption.

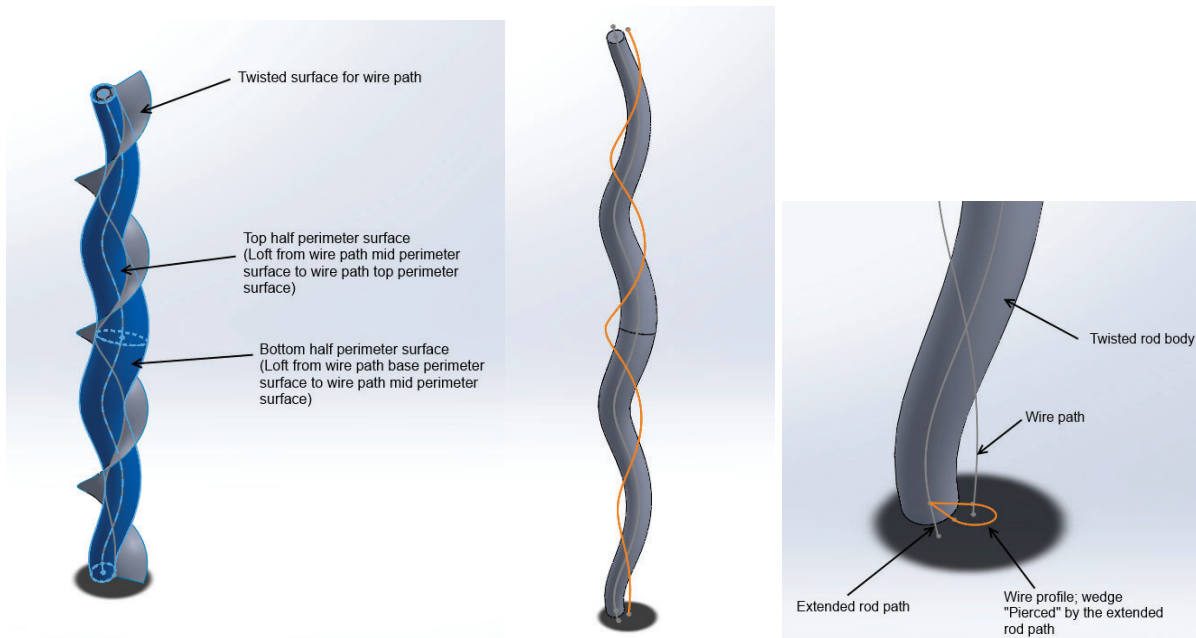


**Figure 6. Wire Path Perimeter (Blue) and Twisted (Grey) Surfaces (Steps 5 and 6, left), Wire Path (Orange, Step 7, middle), Wire Sweep Profile Sketch (Orange, Step 8, right) (not to scale)**

A 19-pin assembly of such rods, compressed axially by a factor of 50, is also shown in Figure 7. This is the deformed assembly simulated using the meshing and physics models in subsection 3.2; its simulation

results are given in subsection 5.2. The center, middle and outer ring rods' twist diameters are 0.07mm, 0.13mm and 0.19mm, respectively; this growth pattern is consistent with Refs. [7,8].

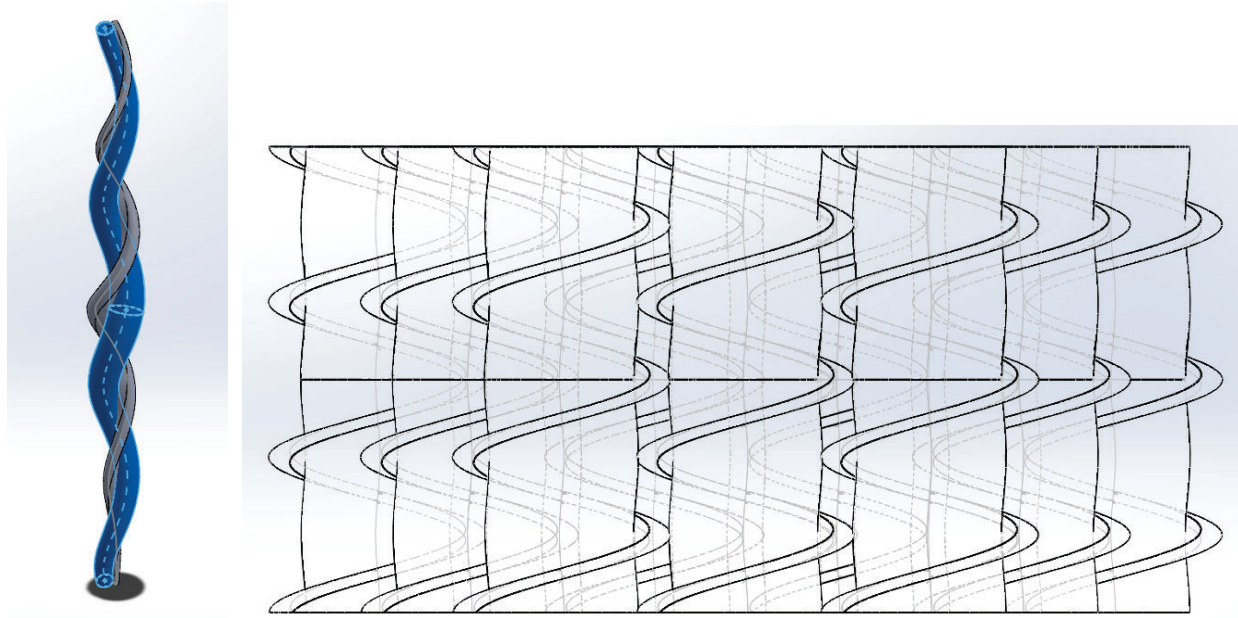


**Figure 7. Single Wire-wrapped Twisted Rod (Blue Rod, Grey Wire, left, not to scale) and 19-pin Assembly Vertical Profile (Compressed Axially by a Factor of 50, right)**

The authors assert that the deformation procedure described in this subsection is more realistic for high burnup fuel than the one described in subsection 2.1, as it matches the non-uniform nature of the experimentally-observed deformations in Refs. [7,8]. It is still conservative compared to the experimental deformations, due to the greater-than-observed average twist of the outermost pins. For this reason, this deformation procedure provides the basis of the deformation penalty factor evaluation methodology proposed in section 4.

### 3. CFD MODELS DESCRIPTION

The two geometries simulated in this work used different fluids and numbers of pins, and therefore two different meshing and physics model combinations are used. Generally, prior to deforming a geometry for CFD simulation, it is important to validate the meshing and physics models on the nominal geometry.

#### 3.1. Meshing and Physics Models for the 127-Pin MYRRHA Fuel Bundle

In order to study the effects of hypothetical deformations on a 127-pin MYRRHA fuel assembly, the Navier-Stokes equations were solved using the STAR-CCM+ v8.06 CFD code. For turbulence, the  $k-\omega$  SST model was used. In these simulations, the working fluid is liquid lead bismuth eutectic, with corresponding temperature dependent physical properties (isobaric specific heat, fluid density, fluid dynamic viscosity), obtained from experimental correlations [12]. For the heat transfer and fluid flow analysis, we include a constant fuel surface heat flux of  $9.24 \times 10^5$  W/m<sup>2</sup> in the active region for all cases. In the cases with deformed fuel pins, the surface area of the deformed fuel rods is slightly larger than in the reference case with straight fuel rods. Consequently, the total heat input imposed is also slightly large since the heat flux imposed on the fuel rods is identical. The active fuel region is between the axial heights of 0.660m and 1.260m. An inlet mass flow rate of 71.4 kg/s is imposed, with inlet fluid

temperature of 543K. At the outlet, Neumann boundary conditions are applied at the outlet of the numerical domain for all velocity components and the pressure. At all solid surfaces, no-slip conditions are applied. For the wire-wraps and the duct, adiabatic thermal boundary conditions are imposed.

The computational domain of such a 127-pin fuel assembly bundle is rather large and complex including the wires. The circular fillet wire simplification, described in section 2 and validated in Ref. [3] is therefore used. The use of a prismatic boundary layer on the solid surfaces is avoided, while in the bulk polyhedral cells were employed to generate the volume mesh. A detailed mesh sensitivity study was performed and presented in Ref. [3] for the 19-pin NACIE bundle (note, that this is different from the 19-pin ORNL bundle discussed in this paper). This sensitivity study used a well-resolved bulk mesh, including boundary layers, in which all  $y^+$  wall treatment model was used, as a reference. An alternative less resolved bulk mesh, and a mesh without any boundary layers, were also used, and compared to the reference solution. The comparison showed hardly any difference between the first two meshes. Employing a mesh without a proper boundary layer, the main flow features were still captured, although differences did occur, e.g., in the prediction of the pressure drop. Nevertheless, the mesh without a boundary layer was selected for the 127-pin fuel assembly simulation, because it has reasonable memory and computation time requirements, at the cost of some accuracy. For greater detail, the reader is referred to Ref. [3]. For the 127-pin geometry, the mesh without boundary layers typically consists of almost 20 million computational cells, as depicted in Figure 8 below.

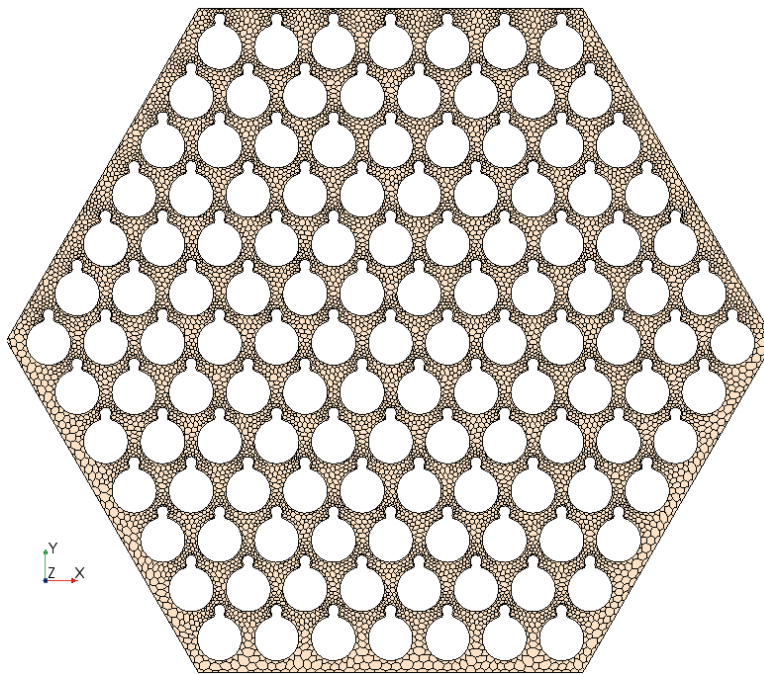


**Figure 8. Typical Mesh in a Cross Plane for a 127-pin Deformed MYRRHA Fuel Assembly Consisting of about 5 Wire Pitches**

### 3.2. Meshing and Physics Models for the 19-Pin ORNL Benchmark Fuel Bundle

The 19-pin ORNL benchmark fuel bundle was meshed and modeled using the methodology validated in Ref. [2]. The working fluid here is liquid sodium, with a 3-turn 36-inch 19-pin bundle. The standard  $k-\varepsilon$  turbulence model with a high  $y^+$  wall treatment is sufficiently accurate to be used for the physics of interest. The average rod surface  $y^+$  in the nominal and fully deformed geometries are 57.3 and 56.6, respectively; both are clearly fully within the log-law region ( $30 \leq y^+ \leq 100$ ). STAR-CCM+ v9.04.009 was used as the CFD code.

The default settings (optimized for liquid water) are, generally, sufficient, with the exception of the minimum allowable wall distance:  $1.0 \times 10^{-10}$  m is recommended.

Unlike in the MYRRHA geometry, the prismatic layer mesher was utilized, which resulted in a large number of cells. To reduce this number, prior to the meshing, the geometry was axially compressed by a factor of 4.0, meshed, and then upscaled again. This scaling factor was chosen to reduce the number of cells required while maintaining accuracy; as with the other meshing settings used, it was verified and validated earlier [2].

A base cell size of 0.2mm was used, with 1 prism layer and a prism layer thickness of 0.09mm. The target surface sizes on non-wire surfaces were chosen to be 100% of the base cell size, and a 50% of base cell target surface size was used on the wire surfaces. This resulted in approximately 26 million mesh cells for the 19-pin geometry, both before and after deformations.

Physically, the problem is again similar to the MYRRHA assembly: an inlet mass flow rate of 2.91 kg/s with a total temperature of 446.77°C was used, with an absolute outlet pressure of 1 atm (zero gauge pressure). The heated length is a 21-inch axial segment 3 inches from the top and 12 inches from the bottom of the 36-inch assembly. The hexagonal duct flat-to-flat inside distance is 34.1mm.

Despite using the prism layer mesher, both the deformed and the nominal geometries meshed in approximately 3 hours each, on a dedicated 2.6GHz meshing machine. The process required up to 60GB of RAM. The most sensitive parameters of the simulation converged within 1000 iterations of the steady state solve.

#### **4. HOT CHANNEL DEFORMATION PENALTY FACTOR EVALUATION METHODOLOGY**

The overall objective of the CFD simulations presented in this paper is to provide an algorithm for LMFBR core designers to follow to quantify penalty factors to use in their simulations, instead of manually deforming their geometries every time. The degree of deformation grows nonlinearly with the radial size of the assembly, and so a fixed penalty factor cannot be used. As a result of the experience obtained with the realistic deformation procedure described in subsection 2.2, the following methodology is proposed:

1. Using the CAD procedures outlined at the beginning of section 2 of this paper, build a model for the nominal assembly of interest.
2. Using the CAD procedures outlined in subsection 2.2, build a model of a fully-deformed assembly of interest.
3. Choose an appropriate meshing and physics model configuration (section 3 is a good starting point, but verification and validation on the nominal geometry may still be required depending on the working fluid, available hardware and other factors).
4. Using this configuration, build and run the CFD simulations for both assemblies. The problem may be larger than the relatively small (20-25 million cells) problems encountered here, depending on the mesh used; at the very least, the radial dimensions have to be preserved, to accurately represent the bypass flows.
5. Post-process the resulting simulations identifying the hottest average outlet subchannel temperature in each geometry.
6. Evaluate the nominal inlet to outlet coolant temperature rise in this subchannel.
7. Evaluate the difference between the hot subchannel's outlet temperatures in both the deformed and the nominal geometries.
8. Evaluate the ratio between this difference in outlet temperatures (step 7), and the nominal inlet to outlet coolant temperature rise in this subchannel (step 6). Add 1.0 to this ratio.

The quantity found in step 8 is the penalty factor. Note, that the outlet subchannel temperature was chosen as the parameter that determines the penalty factor, consistently with subchannel modeling approaches, and as it represents the limiting parameter in SFRs: sodium boiling temperature is much lower than clad melting temperature.

## 5. RESULTS AND ANALYSIS

In this section, the effects of the deformations described in subsections 2.1 and 2.2, as predicted by the CFD models described in subsections 3.1 and 3.2, are quantified and discussed. The penalty factor for the 19-pin ORNL assembly is also calculated, using the methodology from section 4.

### 5.1. 127-Pin MYRRHA Fuel Bundle Results Comparison

The effects of the assumed deformations in a MYRRHA fuel assembly resulting from the uniform twisting due to pre-stressing the wires and placing the rod bundle eccentric in its housing are assessed with CFD. This subsection describes the results of these analyses.

The effects of the deformed fuel rods on the heat transport distribution in the deformed wire-wrapped 127-fuel pin assembly are shown in Figure 9 below. Regions with higher temperatures occur more often for the deformed cases in comparison to the nominal case.

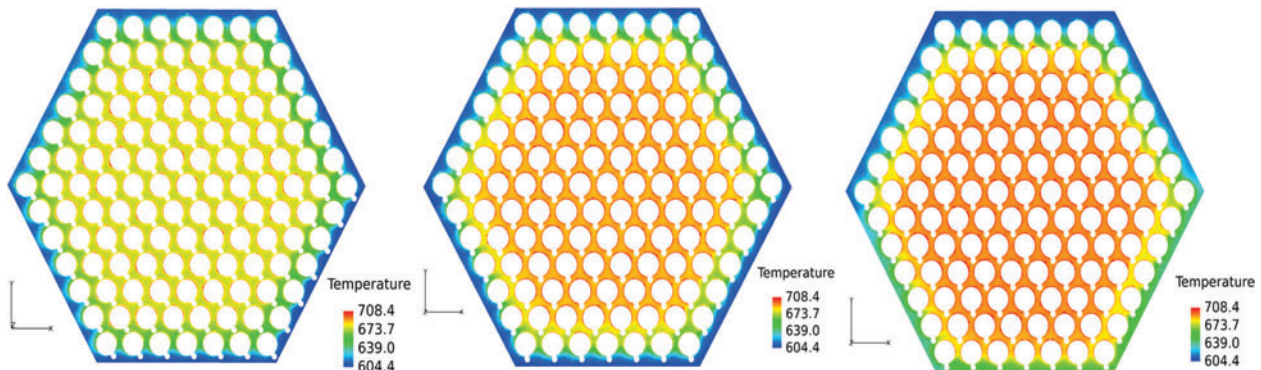


**Figure 9. Temperature Contours at the Height of 1.2m for the Undeformed Case (left), the Deformed Centric Case (middle), and the Deformed Eccentric Case (right) for the 127-pin MYRRHA Fuel Bundle**

The influence of the eccentric placing of the rod bundle with respect to its housing can also be seen in Figure 9. Firstly, it should be mentioned that the velocity field changes significantly for this case, due to the relatively large gap which is formed between the rod bundle and its housing on one side and the small gap on the other side. This leads to a general decrease of the mass fluxes in the central subchannels, and therefore, to higher temperatures.

**Table 1. Comparison of the Undeformed Case, the Deformed Case and the Deformed Eccentric Case for the 127-pin MYRRHA Fuel Bundle**

Case	# cells	$v_{\max}$ (m/s)	$T_{\max}$ (K)
Undeformed	~18.7 M	2.54	722
Deformed Centric	~19.5 M	2.25	746
Deformed Eccentric	~19.4 M	2.68	750

Table 1 summarizes the results quantitatively. It can be seen that the maximum velocity decreases due to the rod deformations in the centric case. In the eccentric case however, the maximum velocity increases due to the large flow area which is created near the rod bundle housing. The maximum temperature on the other hand is for both deformed cases in the same order of magnitude.

## 5.2. 19-Pin ORNL Bundle Results Comparison

The subchannel, pin and crossflow indexing conventions used here are summarized in Figure 10.

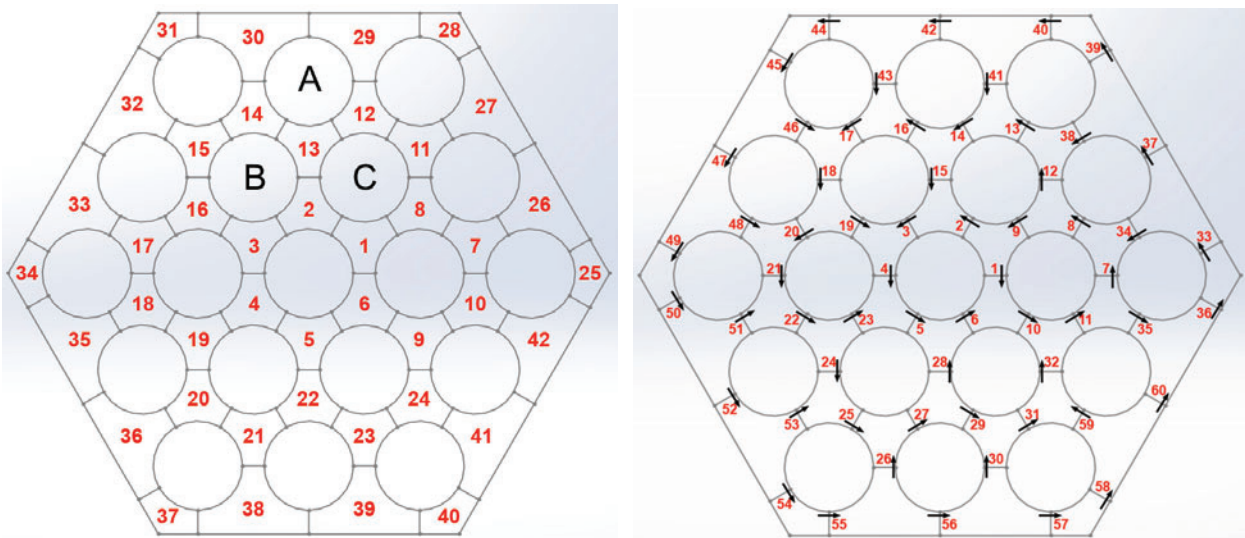


Figure 10. 19-pin Subchannel and Pin (left) and Crossflow (right) Indexing Conventions

Table 2. Comparison of the Subchannel Average Outlet Temperatures for the 19-pin ORNL Fuel Bundle

Subchannel	Subchannel Average Outlet Temperature [K]					
	I	II	III	IV	V	VI
1	837.15	843.04	843.17	843.57	838.45	838.88
2	836.61	844.04	842.80	843.41	838.29	838.72
3	835.87	844.20	841.48	842.05	836.81	837.23
4	838.26	845.86	843.29	843.56	838.42	838.61
5	840.93	<b>847.92</b>	846.35	846.72	841.14	841.46
6	840.23	846.90	844.99	845.56	840.08	840.48
21	829.83	836.19	832.20	832.02	829.48	829.22
37	772.73	771.38	772.30	772.12	773.25	772.99
39	794.93	792.63	792.88	792.39	794.14	793.81

Six different 19-pin cases were analyzed: (I) nominal, (II) fully deformed, (III) deformed duct and 1 outer pin (pin A), (IV) deformed duct with 2 mid-ring and one outer pins (pins A, B and C), (V) nominal duct and 1 outer deformed pin (pin A), (VI) nominal duct and 2 deformed mid-ring and one outer pins (pins A, B and C). In all cases, subchannel 5 was shown to be the limiting one; these results are summarized quantitatively in Table 2 above. All 42 subchannels were looked at, and the results for the hottest ones, as well as several additional channels for comparison, are presented here.

The average outlet temperatures before and after the full deformation were computed to be 802.9K and 803.7K, respectively. This corresponds to a difference of 0.8K, or 0.10%. For other geometries, the error is even less. These differences are clearly very small, therefore the analysis passes the outlet average

temperature sanity check. Based on these observed results, and the methodology outlined in section 4, the calculated penalty factor is 1.058, or 5.8%.

It is also illustrative to look at the changes in the crossflow mass fluxes as a result of deformations. To quantify them, the crossflow mass fluxes in the top 3 inches of the heated section (between  $y = 30\text{in}$  and  $33\text{in}$ ) were studied. Figure 11 below illustrates the computed changes for the two most affected cases. Here we can see, that the deformations reduced most crossflows, except several inner ones. The largest fractional changes occur near corners, where there was, in the nominal geometry, virtually no crossflow. On average, 11.4% less crossflow occurs in Case II, compared to the nominal geometry.

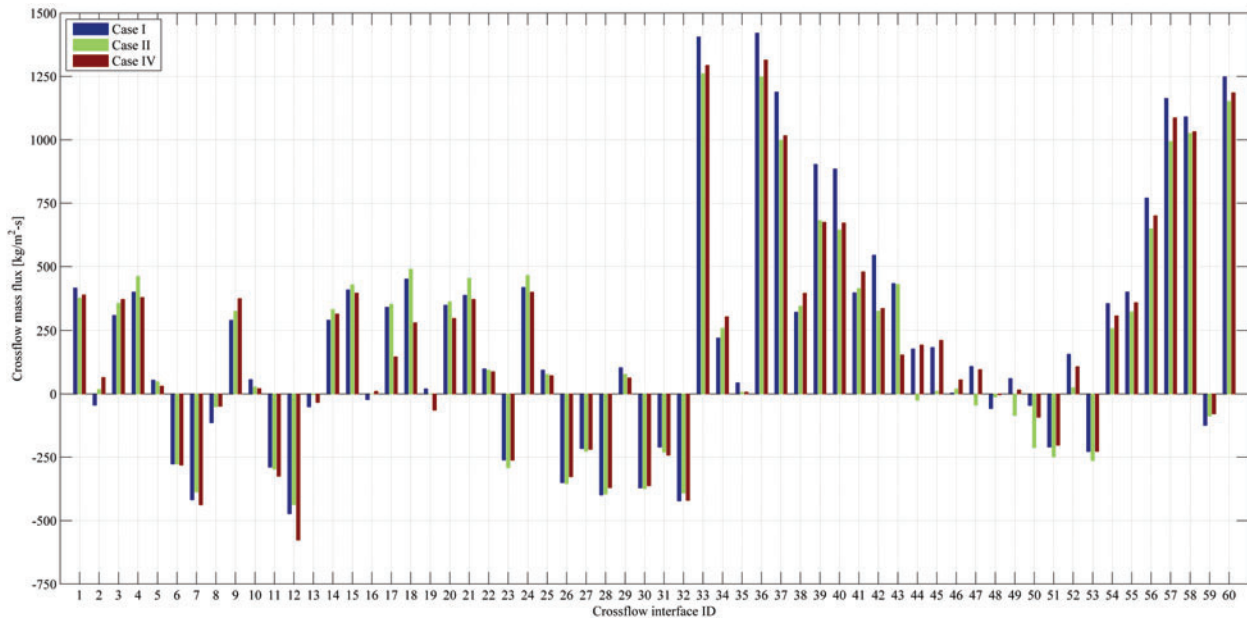


**Figure 11. 19-pin Crossflow Mass Fluxes at the Top 3 Inches of the Heated Section**

Overall, this analysis demonstrated that, as expected, the innermost subchannels are the most affected, and the non-boundary subchannels see a higher flow, and therefore lower temperatures. Horizontal mass transfer is affected more severely than fluid temperatures. These findings make sense: the deformation and the expansion of the duct creates a slight bypass along the duct walls (less so for corners), while the deformation of the inner rods reduces the amount of working fluid available to the rods, and impedes mixing, which increases the outlet temperature.

## 6. CONCLUSIONS AND OUTLOOK

The simulations using a hypothetical deformation of a MYRRHA fuel assembly show the effects of twisting due to pre-stressing the attached wires, and the eccentric positioning of the rod bundle in its housing. Overall, the effect of the deformed fuel rods on the flow field is significant when compared with a reference case containing straight rods. The slight twist of the rods induced by the pre-stressed wires leads to an increase in maximum temperature in the rod bundle interior. For the eccentric case the maximum velocity increases due to the large gap which is formed between the rod bundle and its housing. However, the maximum temperature remains in the same order of magnitude as in the centric deformed case. Such detailed results of the three dimensional flow and heat transport in a fuel assembly provide important input and new insights to the reactor designers. In the near future, the intention of the MYRRHA designers is to simulate the deformations at higher burnup, e.g. through coupling the results of CFD simulations with a structural integrity code.

The 19-pin simulations produced a clear, explicit set of step-by-step procedures to use when forming a limiting deformed LMFR geometry for use in CFD simulations. A step-by-step methodology was proposed to quantify the results of such simulations, to then implement them in subchannel or systems analysis. An example hot channel penalty factor of 5.8% was computed for a test geometry; it is expected that this factor will be of approximately the same magnitude for most SFR and LMFR geometries.

## ACKNOWLEDGMENTS

The MIT portion of this work was sponsored by TerraPower, LLC, which is gratefully acknowledged. The Dutch contribution of the work described in this paper was funded by the Dutch Ministry of Economic Affairs and is performed in a close collaboration between NRG and the MYRRHA design team at SCK•CEN in Belgium.

## REFERENCES

1. F. Roelofs, V.R. Gopala, S. Jayaraju, A. Shams and E. Komen, "Review of Fuel Assembly and Pool Thermal Hydraulics for Fast Reactors," *Nucl. Eng. Des.*, **265**, pp. 1205-1222 (2013).
2. J.W. Fricano and E. Baglietto, "A Quantitative CFD Benchmark for Sodium Fast Reactor Fuel Assembly Modeling," *Ann. Nucl. Energy*, **64**, pp. 32-42 (2013).
3. V.R. Gopala, H. Doolaard, V. Sanna and F. Roelofs, "Detailed Investigation of Flow Through Wire-wrapped Fuel Assemblies Using Computational Fluid Dynamics," *Proceedings of THINS 2014 International Workshop*, Modena, Italy, January 20-22, (2014).
4. M.H. Fontana, R.E. MacPherson, P.A. Gnadt, L.F. Parsly and J.L. Wantland, "Temperature Distribution in the Duct Wall and at the Exit of a 19-Rod Simulated LMFBR Fuel Assembly (FFM Bundle 2A)," *Nucl. Technol.*, **24**(2), pp. 176-200 (1974).
5. H.A. Abderrahim, "Multi-purpose hYbrid Research Reactor for High-tech Applications a Multipurpose Fast Spectrum Research Reactor," *Int. J. Energ. Res.*, **36**(15), pp. 1331-1337 (2012).
6. ESNII, "A contribution to the EU Low Carbon Energy Policy: Demonstration Programme for Fast Neutron Reactors," SNETP, (2010).
7. K. Katsuyama, T. Nagamine, S.-I. Matsumoto and M. Ito, "Application of X-Ray Computer Tomography for Observing the Deflection and Displacement of Fuel Pins in an Assembly Irradiated in FBR," *J. Nucl. Sci. Technol.*, **40**(4), pp. 220-226 (2003).
8. K. Katsuyama, T. Nagamine, S.-I. Matsumoto and S. Sato, "High Energy X-Ray CT Study on the Central Void Formations and the Fuel Pin Deformations of FBR Fuel Assemblies," *Nucl. Instrum. Meth. B*, **255**(2), pp. 365-372 (2007).
9. E. Baglietto, J.W. Fricano and E. Sosnovsky, "CFD Activities in Support of Thermal-hydraulic Modeling of SFR Fuel Bundles," *Proceedings of The 10<sup>th</sup> International Topical Meeting on Nuclear Thermal-Hydraulics, Operation and Safety (NUTHOS-10)*, Okinawa, Japan, December 14-18, (2014).
10. W.D. Pointer, J. Thomas, T. Fanning, P. Fischer, A. Siegel, J. Smith and A. Tokuhiko, "RANS-Based CFD Simulations of Sodium Fast Reactor Wire-wrapped Pin Bundles," *Proceedings of The International Conference on Mathematics, Computational Methods & Reactor Physics (M&C 2009)*, Saratoga Springs, NY, USA, May 3-7, (2009).
11. K.D. Hamman and R.A. Berry, "A CFD Simulation Process for Fast Reactor Fuel Assemblies," *Nucl. Eng. Des.*, **240**(9), pp. 2304-2312 (2010).
12. OECD/NEA, "Handbook on Lead-Bismuth Eutectic Alloy and Lead Properties, Materials Compatibility, Thermal-Hydraulics and Technologies," (2007).